



Project acronym:	GeoHex		
Project title:	Advanced material for cost-efficient and enhanced heat exchange performance for geothermal application		
Activity:	LC-CS3-RES-1-2019-2020 Developing the next generation of renewable energy technologies		
Call:	H2020-LC-CS3-2019-RES-TwoStages		
Funding Scheme:	RIA	Grant Agreement No:	851917
WP1	Requirement analysis and project mapping		

D1.3 Ideal flow boiling surface for ORC fluid

Due date:	29/02/2020				
Actual Submission Date:	28/02/2020				
Lead Beneficiary:	TWI				
Main authors/contributors:	Imran Bhamji				
Dissemination Level¹:	PU				
Nature:	Others				
Status of this version:		Draft under Development			
		For Review by Coordinator			
	X	Submitted			
Version:	V1				
Abstract	This deliverable reports on the identification of the characteristics of optimum surfaces for ideal flow boiling heat transfer related to ORC working fluid.				

REVISION HISTORY

Version	Date	Main Authors/Contributors	Description of changes



This project has received funding from the European Union's Horizon 2020 Research and Innovation programme under grant agreement No. 851917

¹ Dissemination level security:

PU – Public (e.g. on website, for publication etc.) / PP – Restricted to other programme participants (incl. Commission services) /

RE – Restricted to a group specified by the consortium (incl. Commission services) / CO – confidential, only for members of the consortium (incl. Commission services)

This project has received funding from the European Union's Horizon 2020 program Grant Agreement No 851917. This publication reflects the views only of the author(s), and the Commission cannot be held responsible for any use which may be made of the information contained therein.

Copyright © 2019-2022, GeoHex Consortium

This document and its contents remain the property of the beneficiaries of the GeoHex Consortium and may not be distributed or reproduced without the express written approval of the Geo-Drill Coordinator, TWI Ltd. (www.twi-global.com)

THIS DOCUMENT IS PROVIDED BY THE COPYRIGHT HOLDERS AND CONTRIBUTORS "AS IS" AND ANY EXPRESS OR IMPLIED WARRANTIES, INCLUDING, BUT NOT LIMITED TO, THE IMPLIED WARRANTIES OF MERCHANTABILITY AND FITNESS FOR A PARTICULAR PURPOSE ARE DISCLAIMED. IN NO EVENT SHALL THE COPYRIGHT OWNER OR CONTRIBUTORS BE LIABLE FOR ANY DIRECT, INDIRECT, INCIDENTAL, SPECIAL, EXEMPLARY, OR CONSEQUENTIAL DAMAGES (INCLUDING, BUT NOT LIMITED TO, PROCUREMENT OF SUBSTITUTE GOODS OR SERVICES; LOSS OF USE, DATA, OR PROFITS; OR BUSINESS INTERRUPTION) HOWEVER CAUSED AND ON ANY THEORY OF LIABILITY, WHETHER IN CONTRACT, STRICT LIABILITY, OR TORT (INCLUDING NEGLIGENCE OR OTHERWISE) ARISING IN ANY WAY OUT OF THE USE OF THIS DOCUMENT, EVEN IF ADVISED OF THE POSSIBILITY OF SUCH DAMAGE

Document: D1.3 Ideal flow boiling surface for ORC

Version: 1.0

Date: 28 February 2020

CONTENTS

1. EXECUTIVE SUMMARY	4
2. OBJECTIVES MET	4
3. SEARCH METHODOLOGIES	4
4. BOILING HEAT TRANSFER	5
4.1 BACKGROUND.....	5
4.2 METHODS TO INCREASE HEAT TRANSFER PERFORMANCE.....	6
4.2.1 Overview	6
4.2.2 Surface roughening	6
4.2.3 Macro-finned surfaces	6
4.2.4 Foams and meshes.....	6
4.2.5 Micro-fins and channels.....	7
4.2.6 Nano-structures	7
4.2.7 Wettability	7
4.3 QUANTIFICATION OF HEAT TRANSFER ENHANCEMENTS.....	8
5. ENHANCEMENT METHODS SPECIFIC TO GEOHEX.....	10
5.1 IRON DOPED Al ₂ O ₃ AND/OR TiO ₂ COATINGS.....	10
5.2 MULTI-WALLED CARBON NANOTUBE COATINGS	11
5.3 CuO SUSPENSION SPRAY COATINGS.....	12
5.4 Ni-P/Ni-P-PTFE COATINGS	14
5.5 AMORPHOUS METAL COATINGS	14
6. CORRELATIONS FOR POOL AND FLOW BOILING	15
7. IMAGING METHODS FOR SIMULATION VALIDATION.....	16
8. CONCLUSIONS	17
9. REFERENCES	18

1. EXECUTIVE SUMMARY

The GeoHex project aims to develop coatings to enhance boiling heat transfer performance. The current document reviews the critical factors affecting boiling heat transfer, including surface morphology and roughness, microstructure, chemistry and thermal conductivity, among others, and identifies the state-of-the-art (SOA) to enhance heat transfer coefficient (HTC) and critical heat flux (CHF).

Section 4 of the review focuses on SOA research and practice on enhancement of HTC and CHF, while Section 5 is a more detailed review of enhancement techniques that will be used in GeoHex. Section 6 discusses correlations between HTC and CHF and thermocouple data as well as bubble dynamics parameters, determined through image acquisition systems and modelling. Section 7 discusses the rationale behind imaging aspects, and is common to both boiling and condensation, covered in D1.4, experiments.

2. OBJECTIVES MET

The deliverable helps meet the following work package objectives:

- To characterise the ideal boiling surface for low surface tension fluid

3. SEARCH METHODOLOGIES

Literature searches were mainly undertaken using Scopus, and the search terms are listed in Table 1. These searches were supplemented with relevant papers provided by the research partners. It is noted that broad searches, for example Index 1 in Table 1, resulted in too many hits for assessment using manual techniques, and therefore the search terms were narrowed so that a more manageable number of hits was obtained. Inevitably, this might have resulted in papers of potential relevance not being reviewed in this report.

Table 1 List of search terms

Index	Search String	Hits
1	TITLE-ABS-KEY (boiling AND coat*)	3,068
2	TITLE-ABS-KEY (boiling AND coat* AND geothermal)	7
3	TITLE-ABS-KEY (boiling AND coat* AND (geofluid* OR "geo fluid*"))	0
4	TITLE-ABS-KEY (boiling AND coat* AND geo* AND NOT geomet*)	25
5	TITLE-ABS-KEY (boiling AND coat* AND ("organic rankine" OR orc))	3
6	TITLE-ABS-KEY ((cuo OR "copper oxide*") AND ((thermal W/2 spray*) OR (suspension W/2 spray*) OR (flame W/2 spray*) OR (plasma W/2 spray*) OR (hvoft) OR ("high velocity oxy*") OR (spray W/2 pyrolysis)))	420
7	TITLE-ABS-KEY ((cuo OR "copper oxide*") AND boiling AND ((thermal W/2 spray*) OR (suspension W/2 spray*) OR (flame W/2 spray*) OR (plasma W/2 spray*) OR (hvoft) OR ("high velocity oxy*") OR (spray W/2 pyrolysis)))	1
8	TITLE-ABS-KEY ((cuo OR "copper oxide*") AND (nanoporous OR *porous) AND ((thermal W/2 spray*) OR (suspension W/2 spray*) OR (flame W/2 spray*) OR (plasma W/2 spray*) OR (hvoft) OR ("high velocity oxy*") OR (spray W/2 pyrolysis)))	28
9	TITLE-ABS-KEY (("carbon nano*") boiling)	308
10	TITLE-ABS-KEY ("carbon nano*" AND boiling AND ("chemical vapour" OR "chemical vapor" OR cvd))	30
11	TITLE-ABS-KEY ((fe OR iron) AND dop* AND boiling)	52
12	TITLE-ABS-KEY ((fe OR iron) AND dop* AND coating)	1756
13	TITLE-ABS-KEY ((amorphous OR glass) AND metal* AND corrosion)	5685
14	TITLE-ABS-KEY ((amorphous OR glass) AND metal* AND corrosion AND (tantalum OR ta) AND ("physical vapo*" OR pvd))	1
	(TITLE-ABS ((amorphous OR glass) AND metal* AND corrosion AND (tantalum OR ta) AND (silicon OR si) AND ("physical vapo*" OR pvd OR (magnetron W/1 sputt*))))	0

Date: 28 February 2020

Index	Search String	Hits
15	TITLE-ABS-KEY ((amorphous OR glass) AND metal* AND corrosion AND ("physical vapo*" OR pvd))	55
16	TITLE-ABS-KEY ((amorphous OR (metal* W/2 glass)) AND corrosion AND ("physical vapo*" OR pvd OR (magnetron W/1 sputter*)))	464
17	TITLE-ABS-KEY ((amorphous OR glass) AND metal* AND corrosion AND ("physical vapo*" OR pvd) AND (boiling OR condensation))	0
18	TITLE-ABS-KEY (("Ni-P" OR nickel W/2 phosphorus) corrosion)	456
19	TITLE-ABS-KEY (("Ni-P" OR nickel W/2 phosphorus) (ptfe OR polytetrafluoroethylene) corrosion)	7
20	TITLE-ABS-KEY ((fe3o4 OR "iron oxide*") AND (nanoporous OR *porous) AND ((thermal W/2 spray*) OR (suspension W/2 spray*) OR (flame W/2 spray*) OR (plasma W/2 spray*) OR (hvof) OR ("high velocity oxy*") OR (spray W/2 pyrolysis)))	24
21	TITLE-ABS-KEY ((nanoporous OR *porous) AND ((thermal W/2 spray*) OR (suspension W/2 spray*) OR (flame W/2 spray*) OR (plasma W/2 spray*) OR (hvof) OR ("high velocity oxy*") OR (spray W/2 pyrolysis)))	2418
22	TITLE-ABS-KEY ((tio2 OR titania OR titanium W/3 oxide*) AND (nanoporous OR *porous) AND ((thermal W/2 spray*) OR (suspension W/2 spray*) OR (flame W/2 spray*) OR (plasma W/2 spray*) OR (hvof) OR ("high velocity oxy*") OR (spray W/2 pyrolysis)))	64

4. BOILING HEAT TRANSFER

4.1 Background

Boiling is a type of phase change heat transfer that occurs in the evaporator of a geothermal organic Rankine cycle (ORC) heat exchanger. Phase change can dramatically enhance heat transfer, compared with single phase, as latent heat is much larger than sensible heat, while the associated large changes in specific volume can also enhance convective heat transfer (Attinger, 2014). Boiling can be classified into pool or flow boiling; flow boiling, where the fluid is forced to move over the heated surface, is most relevant to heat exchangers (Bejan, 2003). Different forms of boiling are encountered with different levels of subcooling, ΔT , which is the difference between the temperature of the heated surface and the saturation temperature.

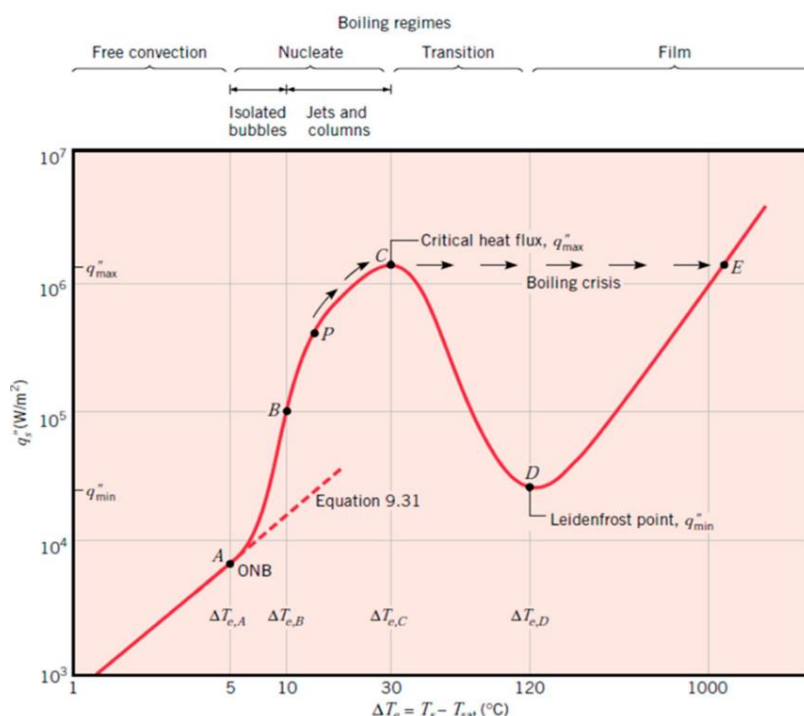


Figure 1 Boiling heat transfer curve, with heat flux on the y-axis and subcooling on the x-axis (Khan, 2018).

The highest heat flux, critical heat flux (CHF), is achieved at the temperature, T_c , in the nucleate boiling regime, where vapour bubbles form at the heat transfer surface and are carried into the fluid stream. If the level of subcooling is increased, above the level for CHF, local vapour layers are formed that provide insulation and reduce heat transfer. A dramatic rise in temperature at the heat transfer surface, known as the 'boiling crisis', can then occur as the heat flux remains, while the heat transfer coefficient has deteriorated. This temperature rise can have a detrimental impact on the heat transfer surface, leading to burnout, and therefore only the region of the curve to the left of the CHF, Figure 1, is of engineering importance. In order to enhance heat transfer performance it is therefore required to increase CHF as well as T_c .

4.2 Methods to increase heat transfer performance

4.2.1 Overview

Heat transfer enhancement techniques can be classified as active, passive or compound. Active techniques require external power to increase fluid mixing and include methods such as surface and/or fluid vibration (stirring, sonication), application of electrostatic fields to dielectric fluids, or application of magnetic fields (Thulukkanam, 2013). The requirement for external power limits use of these techniques in many cases (Sheikholeslami, 2015), while their application is also costly. Passive techniques include surface modifications, e.g. coatings or texturing, as well as devices inserted into the flow stream to produce secondary flows, which support high heat transfer coefficients. Sheikholeslami (2015) provides a review of heat transfer enhancement using inserted devices and macro-scale changes in geometry. The main focus of this review, and the focus of the GeoHex project, will be related to micro/nano-scale surface modification for enhancement of heat transfer. These techniques can increase heat transfer and delay CHF for pool as well as flow boiling. For flow boiling, high flow velocities can also be used to delay CHF as vapour bubbles can be swept away from the surface instead of forming insulating vapour layers.

4.2.2 Surface roughening

Surface roughness enhances heat transfer by increasing surface area, which tends to increase the number of nucleation sites thereby generating a greater number of bubbles (Attinger, 2014). Surface roughening can be achieved by mechanical methods, such as machining, sandpapering etc, and/or heat treatment and chemical etching processes, which can produce more complex features. In general, the features produced using mechanical and chemical processes are random. Data from different researchers on the effect of surface roughness on CHF were compiled by Vlachou (2015) and there was a general trend of increasing CHF with roughness. However, the roughening method also appeared to play a role in the CHF, and this was likely because the microgeometry of the roughness features was also important and was not captured by typical roughness measurements, for example root mean square (rms). It has been noted that large cavities filled with liquid are poor bubble generation centres and do not enhance CHF, even if they do increase roughness (Pioro, 2004). Therefore microgeometry elements are required that do not fill with liquid after bubble departure, such as steep walled or re-entrant cavities.

4.2.3 Macro-finned surfaces

Macro-finned surfaces, with fin widths in the range of ~1-3mm, and heights <5mm, are thought to be effective in enhancing heat transfer, and a 200% enhancement in CHF was reported (Zhong, 2015) for milled copper surfaces in deionised water, relative to a flat surface. The design of structures, for optimal performance, is dependent on a number of aspects, including working fluid, fin height and spacing, surface orientation and pressure. Systematic studies are therefore required to provide design guidelines for optimum structures (Liang, 2019).

4.2.4 Foams and meshes

Various porous media have been used to enhance heat transfer, and an increase in CHF was reported for honeycomb porous ceramic layers (Mori, 2017a). The enhancement was attributed to capillary wicking, which is reported to be crucial in maintaining a wetted surface at high vapour production rates, as well as rewetting dry patches (Rahman, 2014). In addition to wicking, the

increased surface area of porous structures also contributed to the enhanced performance. Porous foams have also been reported to improve heat transfer performance, (Yang, 2010), with improvements of 2 to 3 times, compared with plain surfaces.

Metal foams have also been used to enhance heat transfer and it was demonstrated, (Yang, 2010), that copper foams, welded onto copper substrates, can enhance heat transfer coefficients by 2 to 3 times, compared with a plain surface. An optimum value of pores per inch (ppi), of 60, was determined, and at small ppi values there was a decrease in the heat flux that could be dissipated at a wall superheat, while with large ppi values, bubble nucleation sites increase, but there was a large resistance to vapour release. The thickness also had an impact on performance, with an optimal value determined, that was dependent on ppi.

4.2.5 Micro-fins and channels

Heat transfer can also be enhanced by the separation of liquid and vapour flow paths, as the blocking of liquid replenishment by escaping vapour can degrade heat transfer performance. On a global scale this can be achieved by using a pumpless loop (Mukherjee, 2003), while on a more micro-scale bi-conductive coatings have been produced, with rows of low conductivity epoxy and high conductivity copper, exposed on the heat transfer surface. The superheat at the copper layers is much higher than at the epoxy layers, resulting in vapour flow from the copper layers, with replenished cooler liquid from above the epoxy layers (Rahman, 2015).

Re-entrant geometries have also proved useful for heat transfer enhancement, and three modes of heat transfer were identified with these surfaces:

- 'Dried up mode': where cavities were filled with vapour and boiling took place outside the cavities.
- 'Suction-evaporation mode': where vapour release causes suction of liquid into inactive cavities, from a network of non-isolated cavities. This mode provided the best heat transfer performance.
- 'Flooded mode': where cavities are flooded with liquid with few active nucleation sites.

The cavity state, for re-entrant cavities is thought to be related to the superheat, the radius of the neck and the inverted radius of the cavity (Attinger, 2014).

4.2.6 Nano-structures

A number of researchers have studied the influence of carbon nano-tubes (CNTs) and wires deposited onto heat transfer surfaces. The deposition technique was normally chemical vapour deposition (CVD), and heat transfer enhancement has been mainly attributed to capillary wicking (Liang, 2019), as well as increased surface area. The nano-topographies are thought to be susceptible to blockages, causing decay in heat transfer performance with time (Liang, 2019).

4.2.7 Wettability

Hydrophilic surfaces, with static contact angles (CA) of $< 90^\circ$, as well as superhydrophobic surfaces, with CA of $> 150^\circ$, can increase heat transfer. This is because there are competing influences, related to increased bubble nucleation density with hydrophobic surfaces, but also lack of wicking and rewetting. The initial wetting state of hydrophobic surfaces is also thought to influence the heat transfer performance. It was found that film boiling was achieved when boiling was initiated from a Cassie-Baxter state, where air is trapped in the asperities/geometry of a featured surface, while nucleate boiling was achieved when boiling was initiated from the Wenzel state, where the surface was completely wetted (Allred, 2018).

4.3 Quantification of heat transfer enhancements

A number of reviews of surface modification for the enhancement of boiling heat transfer have been completed recently (Khan, 2018; Mori, 2017b; Liang, 2019), and some of these have included summaries of the heat transfer enhancements reported in the reviewed papers. These summary tables are reproduced in Tables 2a 2b and 2c.

Table 2a Nanoparticle coatings for boiling heat transfer enhancement (Khan, 2018)

S. No	Substrate	Type of Nanoparticles	Preparation Techniques	Working Fluid	Enhancement
1	Nickel wires	Silica nanoparticles	Layer by layer (lbl) assembly method	Water	100%
2	Cu plate	Al_2O_3	Nanofluid boiling	Water	Enhanced
3	Cu	TiO_2	Nanofluid boiling	Distilled water	HfC by 38%
4	Cu	Al, Cu, Ag and diamond particles	Dipping and backing	FC-72	Enhancement: up to 4.5 times in HfC and 2 times in CHF
5	Platinum	Diamond	DOM coating	FC-72	\approx 100% CHF enhancement
6	Cu plate	ZrO_2	Nanofluid boiling	Water	Enhanced
7	Stainless steel disk	ZnO	Electrophoretic deposition	ZnO-propylene	200%
8	untreated rectangular heater	Al_2O_3	Nanofluid boiling	Water	32%
9	Nicr wire	SiO_2	Nanofluid boiling	Water	Enhanced by 3 times
10	Aluminum and copper	Cu, Al, bronze, and corundum particles	Plasma sprayed coating	Freon	Max. Enhancement up-to 32%
12	Small horizontal tube with diameter 4 to 6.5 mm	Al_2O_3	Boiling nanofluid	Water	Enhanced
13	Pt Wire And Heater(Square)	Al_2O_3	Nanofluid Boiling	Water	CHF By 200%
14	Cu machined surface and polished surface	Al_2O_3	Nanofluid Boiling	water	Enhancement up-to: 7% in CHF, and 37% in HfC
15	Cu surface	Cu- Al_2O_3	Electrochemical deposition	DI water	Enhancement up-to 68% in CHF, and 260% in HfC
16	Cu surface	GO and Cu particles coating	Screen printing and electrodeposition	water	Enhancement up-to: 1.8-fold in CHF, and 2.4-fold in HfC
17	Cu surface	Micro-nanostructured surfaces	Femtosecond laser processing	N-pentane	Enhancement up-to 60% in CHF, and 300%in HfC
18	Cu surface	TiO_2 nanoparticles film	Electron beam evaporation method	R134a	HfC increased by 87.5%
19	Cu surface	SiO_2 nanoparticles film	Electron beam evaporation technique	water	HfC increased by 80%
20	Cu surface	Cu- TiO_2 nanocomposite	Electrocodeposition	DI water	CHF increased up to 92%
21	Flat Stainless steel surface	Al_2O_3 nanoporous surface	Electrophoretic deposition	Pure SES36 fluid	Maximum HfC increased by 76.9%

Table 2b Porous coatings for boiling heat transfer enhancement (Khan, 2018)

S. No	Substrate	Coated Material	Geometry	Coating Technique	CHF
1	Tin	Metallic copper foam	V shaped grooved metallic foam with porosity of 0.95 and thickness 2 and 4 mm.	Binding by Welding	Enhancement of CHF 1.5 times and HTC 3 times.
2	Porous structure of cu particles	Cu particles of 250 μm to 400 μm	Uniform Thick porous structures and pillars porous structures	Sintering	CHF 450 W/Cm ² , 3 times higher to corresponding plain surface. And HTC 3 times higher
3	Al And Cu	ZnO	ZnO Nanostructured on Substrate	Micro Reactor-Assisted-Nanomaterial-Deposition (MAND)	CHF: 82.5 W/Cm ² , 3.5 Times Enhancement
4	Silicon	Cu and Si	Nanowires on Cu and Si Substrate	Electroplating and Etching	CHF: 192 And W/Cm ² , Enhanced By 100%.
5	Copper	Cu Particles	Porous coating of Cu particles on Cu Substrate	Brazing	CHF: 2.1-fold
6	Cu	Cu Particles	Micro-porous coating	Sintering	CHF: 4.5 Times Higher
7	Cu	Cu Particles	Hierarchical micro-porous structures	-	CHF Enhancement: 412%
8	Si	Diamond Particles	Diamond Based Micro-Porous coating on Si Heater	Diamond-Omega Bond-Acetone (DOA) Coating	47 W/Cm ² , up to 60% Enhancement.
9	Cu	Alumina	Porous alumina coating in a mini channel	Spray pyrolysis coatings	28.3% enhancement in heat flux
11	Cu Chip	-	Porous Layers on micro-channels/Fins Top	Two step electrodeposition process	Up-to 3250 KW/m ²
12	Cu	Al ₂ O ₃ -TiO ₂	Nanostructured porous surface	Facile hot-dip galvanizing/dealloying process	CHF and HTC increased by 52.39% and 44.11%.
13	Cu	Porous graphite	Porous surface with pores ranges from 1 to 100 μm .	-	Enhanced HTC by 57% and CHF 15%
14	Cu	Porous coating	Porous coating on copper fin top	Electrodeposition	Maximum CHF enhancement of 270%
15	Stainless steel foil	micro-cavities	Multi-scale micro-cavities (0.2 to 10 μm)	Laser-processed	HTC increased by 3.7 factor
16	Cu	Cu micro particles	Micro-nano bi-porous surface	Hydrogen bubble template deposition method	HTC increased by 4.8 times
17	Si	Boron nitride	Film coating	Spray coating	Maximum HTC enhancement of 160%
18	Cu tube	Ag particles	Porous coating	Powder flame spraying technique	Maximum HTC increased by 2 times

Table 2c Hydrophilic and hydrophobic coatings for boiling heat transfer enhancement (Khan, 2018)

S. No	Substrate	Coating Material	Coating Technique	Nature (Hydrophilic/Hydro-Phobic)
1	Heating surface	Nickel with polytetrafluoroethylene (PTFE) particles	Electrolytic nickel coating with PTFE particles	Hydrophobic
2	Ni Wires of 0.25 mm	PAH/SiO ₂	Layer by layer assembly method	Hydrophilic, hydrophobic and super hydrophobic
3	Stainless-steel foil	Polydimethylsiloxane-silica coating	Pulsed Nd: YAG laser	Bipolar (hydrophobic/superhydrophilic patterns)
4	Sapphire substrate	SiO ₂ nanoparticles and monolayer thickness fluoro silane	Layer by layer deposition	Hydrophilic and hydrophobic matrices
5	Cu substrate	Teflon layer (hydrophobic), TiO ₂ (hydrophilic)	Hydrophobic: photolithography. Hydrophilic by two step process: layer by layer self-assembly and liquid phase deposition	Hydrophobic, hydrophilic and mixed hydrophobic/hydrophilic
6	Stainless-steel	Silicon oxide and silicon carbide	Pulsed Nd: YAG laser	Hydrophobic and superhydrophobic patterns
7	Copper	Fe-Doped Al ₂ O ₃ -TiO ₂ Composite	Spray coating	Hydrophilic
8	Glass	Octadecyltrichlorosilane (OTD) to add hydrophobic layer	Immersion in ots mixture	Hydrophilic and hydrophobic
9	Copper	Cuprous and cupric oxides	Using alkali solution	Hydrophilic surfaces
10	TiO ₂	Photo-induced wettability	Ultraviolet light irradiation	Enhanced wettability
11	Metal tube	FeCrAl and Cr	Direct current magnetron sputtering	Hydrophilic and superhydrophilic

As can be seen from the above tables, most of the studies mentioned in the summaries are related to water as the working fluid, or other media not typically used as ORC working fluids (Calise, 2018). It is noted that the use of water as the working fluid can result in heat fluxes an order of magnitude higher than for other refrigerants, related to its high boiling point and latent heat of vaporisation (Vlachou, 2015). In relation to boiling studies with relevant refrigerants, wire meshes have been demonstrated to improve heat transfer performance, in R141b, with the commencement of boiling at lower superheats and increases of CHF by 40% (Franco, 2006), relative to a smooth surface. Critical heat flux enhancement of 20% was reported for a copper vacuum plasma sprayed coating in HCFC123 (Asano, 2009).

5. ENHANCEMENT METHODS SPECIFIC TO GEOHEX

5.1 Iron doped Al₂O₃ and/or TiO₂ coatings

Iron doped TiO₂ coatings are of interest for a number of applications, including gas sensors (Effendi, 2012) and photocatalysis (Lin, 2012). The doping of TiO₂ and/or Al₂O₃ with iron, can be used to produce hydrophilic coatings (Weng, 2005). Therefore, such coatings might also be of interest in heat transfer applications. Only a few papers have studied the impact of doping on hydrophilicity, and the resulting heat transfer performance, and it was found that the CHF can be increased by up to 30% for Al₂O₃-TiO₂ composite coatings doped with iron, with demineralised water as the working fluid, (Kumar, 2015). Similarly, heat transfer performance was improved by 35%, for ZnO-Al₂O₃ coatings doped with a surfactant (Kumar, 2016). It is thought that the doping of oxides with metal ions, has the effect of increasing porosity and decreasing band gap energy resulting in the hydrophilicity and improved heat transfer performance (Kumar, 2015). It is noted that studies on the hydrophilicity of copper and vanadium doped TiO₂, as well as aluminium doped ZnO have also been conducted (Kumar, 2016), although the studies did not specifically focus on heat transfer performance.

Metal doped metal oxides have been produced using spin coating (Effendi, 2012; Lin, 2012), but the TiO₂-Al₂O₃ composite coatings, which will be developed for GeoHex, have been produced previously using spray pyrolysis (Kumar, 2015). For spray pyrolysis, a precursor solution is injected

Date: 28 February 2020

into a carrier gas and, the precursor as well as carrier gas, are ejected through a spray nozzle into a hot jet stream (e.g. plasma) to coat a substrate.

The same procedure, as described in (Kumar, 2015), will be used as a starting point for this project, as follows. Fe doped TiO₂ precursor solution will be prepared using, butyl titanate (Ti (OC₄H₉)₄) and ferric nitrate (Fe (NO₃)₃), with acetyl acetone (CH₃COCH₂COCH₃) as the stabilizer and ethanol (C₂H₅OH) as the solvent. Butyl titanate, ferric nitrate and acetyl acetone (Butyl titanate-acetyl acetone molar ratio of 2-1) will be dissolved in ethanol. The Fe concentrations will be varied at four levels within, approximately, 0-7.2 at%.

For preparing the alumina precursor solution, two grams of aluminium isopropoxide will be mixed with 1 litre of demineralised water, which will be placed on a magnetic stirrer for 2 hours at room temperature, to form a uniform solution. The pH of the prepared solution will be kept at ~4, by adding controlled amounts of nitric acid solution. Then the solution will be stirred at 80°C until it becomes clear. Finally, Al₂O₃ and iron doped TiO₂ precursor solutions will be mixed to obtain a final molar ratio of 9:5. Prior to the deposition of Fe doped Al₂O₃-TiO₂ composites, the carbon steel substrate will be grit blasted to remove contaminants and enhance roughness, and will then be degreased with acetone.

5.2 Multi-walled carbon nanotube coatings

CNTs have high thermal conductivities and this, together with their nano-finned surfaces, has a beneficial effect on boiling heat transfer performance (Kumar, 2014). There are three widely used processes for the production of single-walled and multi-walled CNTs (SWCNTs and MWCNTs, respectively), namely arc-discharge, laser ablation and chemical vapour decomposition (CVD). SWCNTs consist of a single graphene sheet rolled into a tube structure, while MWCNTs consist of a number of graphene sheets stacked and rolled into a tube structure.

The electric arc discharge method involves establishing a DC discharge between graphite electrodes. Although the rate of synthesis for this technique is high, the process results in uneven consumption of the anode and material build up at the cathode, in only a few minutes, resulting in instability of the arc. This means that it is difficult to scale up the process. Laser ablation involves the vaporisation of a graphite target in a heated furnace through which an inert gas flows. Laser ablation has proved more successful, compared with arc discharge, for the production of high purity nanotubes, but the process has limited scalability as powerful lasers are required, along with a high temperature environment (Kingston, 2003).

CVD involves the pyrolysis of carbon-rich particles, in the gas phase, in the presence of a catalyst. The process is mature and industrially realised for the production of MWCNTs, although the production cost for single walled CNTs is still quite high. This is because the formation energies of SWCNTs are higher than MWCNTs meaning that MWCNTs can be generated at lower temperatures compared with MWCNTs (Wang 2019).

Table 3 Process parameters for the production of CNTs (Manawi, 2018)

Catalyst	Carbon Source/Gas Phase	Temperature (°C)	Product
Co, Ni, Fe/MgO	CH ₄ /H ₂	1000	SWCNTs
Fe/Al ₂ O ₃	C ₂ H ₄ /N ₂ , H ₂	650	MWCNTs
Fe/Al ₂ O ₃	C ₂ H ₄ /N ₂ , H ₂	500–700	MWCNTs
Ni-Cu/Al ₂ O ₃	C ₂ H ₄ /N ₂ , H ₂	850	MWCNTs
Fe/SiO ₂ /Al ₂ O ₃	Propylene/N ₂	-	MWCNTs
Ni/SiO ₂	CH ₄ /Ar	760	SWCNTs
Fe/Al ₂ O ₃	Ethylene/N ₂ , H ₂	550	CNTs
Fe/silica	Acetylene/N ₂ , H ₂	700	CNTs
Fe/Al ₂ O ₃ , SiO ₂ , TiO ₂ or ZrO ₂	CH ₄ /H ₂	650–800	MWCNTs
LaCoO ₃	C ₂ H ₂ /N ₂ , H ₂	675–700	MWCNTs
Co-Mo/SiO ₂	CO	750	SWCNTs
LaCoO ₃	C ₂ H ₂ , CH ₄ /N ₂	700	MWCNTs
Fe ₂ O ₃	CH ₄ /Ar	1000	SWCNTs
Ni-Cu-Al	CH ₄ /N ₂ , H ₂	700–750	CNTs
Fe	C ₆ H ₆ /Ar	750	MWCNTs
Ni/Fe/CO/HZSM-5 Zeolite	Polypropylene (PP), polyethylene terephthalate (PET), polyethylene (PE), Polyvinyl chloride(PVC), PET/Ar, H ₂	400–900	MWCNTs
NiO/HZSM-5 Zeolite	polypropylene (PP)/H ₂	500–800	MWCNTs
Fe	PP,PE, PVC/Ar, H ₂	800	MWCNTs
Si/SiO ₂	CH ₄ /H ₂	900	SWCNTs
Fe ₂ CO/Al ₂ O ₃	C ₂ H ₄ /Ar, H ₂	750	MWCNTs
Si/SiO ₂ /Al ₂ O ₃	C ₆ H ₁₂ /H ₂	750	MWCNTs
Ni	C ₂ H ₂ /H ₂	550	MWCNTs
Si	C ₂ H ₂ /H ₂ , (Fe(CO) ₅	600–750	MWCNTs
Si ₃ N ₄	C ₂ H ₂	800–1000	SWCNTs
Ba/Ca	C ₂ H ₂ /H ₂ , Ar	700	MWCNTs
Fe(CO) ₅	CO	800–1200	SWCNTs
Fe-Mo	CH ₄ /Ar	875	DWCNTs

The process variables for CVD production of CNTs are catalyst type, catalyst particle size, carbon source and reaction temperature. A number of catalyst materials have been used successfully while catalyst particle diameters >3nm are considered necessary for the production of MWCNTs. The transition elements, iron, cobalt and nickel, are the most widely used catalysts because of their high carbon solubility and carbon diffusion coefficients (Wang, 2019). The most common carbon sources include carbon monoxide, ethane, ethylene, acetylene, benzene and xylene. MWCNTs are favoured by temperatures between 600 and 900°C, while SWCNTs are favoured between 900 and 1200°C. As can be seen from Table 3, CNTs have been produced with a wide variety of process conditions (Manawi, 2018), but more work is required to optimise process parameters for optimisation of yield and properties.

Carbon nanotubes, for heat transfer enhancement, have been studied by a number of researchers, and under flow boiling in water, it was found that enhancement levels, as well as the robustness of the enhancement (i.e. performance with time) were higher at lower flow rates (Kumar, 2014; Singh, 2010). The impact of height of aligned MWCNTs on heat transfer performance was studied by Ahn (2009) and it was found that both heights studied gave similar performance in the nucleate boiling regime. The three references discussed in this paragraph utilised CVD for synthesis of MWCNTs, but coatings have also been produced using cold spray (Pialago, 2013) and sintering (Zheng, 2015). Hydrophobic-hydrophilic MWCNTs have also been produced by partially oxidising pristine MWCNTs, with an enhancement in heat transfer performance reported. As with the field more generally, systematic studies of parameter-performance relationships have not been completed and therefore it is difficult to use the prior literature to inform coating development in GeoHex.

5.3 CuO suspension spray coatings

Suspension thermal spraying (STS) is a thermal spray process, which makes use of liquid feedstock that consists of submicrometer or nano-particles suspended in solvents. The solvent is normally water, alcohol or water-alcohol mixtures (Toma, 2010). Conventional thermal spray utilises powder feedstock with typically 10–100µm diameter. The development of STS has its origins in the need to develop nano-structured coatings, a task for which conventional thermal spray is ill-suited, as

Date: 28 February 2020

particles <5µm diameter have poor followability, leading to the clogging of equipment (Aghasibeig, 2019). Nano-structured but micro-scale powders might also be utilised, although there is a tendency for the sintering of the nano-features when the powder/coating is exposed to the high temperatures associated with thermal spraying, leading to much larger features in the coating (Pawlowski, 2008). STS consists of liquid precursors, with typically 5-50wt% solid, being injected into a flame or jet created by a spray torch. The equipment for STS, is broadly similar to that which is used for thermal spray, with the major difference being the equipment used to deliver a liquid feedstock. Therefore, as with thermal spray, different techniques are used to produce the flame or plasma, needed to melt the precursor materials, as discussed below (Sulzer Metco, 2013):

- Flame spray: Where the liquid precursor is injected into a oxygen-fuel flame. The fuel gas can be either acetylene, propane or hydrogen.
- Plasma spray: A high frequency arc is struck between an anode and cathode, which ionises the gas flowing between anode and cathode (typically Ar, or Ar+H₂ mixtures). The liquid precursor is delivered from outside the resultant plasma plume.
- High velocity oxy-fuel (HVOF): Relies on the combustion of an oxygen-fuel mixture in a combustion chamber, and the expansion of this jet at the exit of the spray gun. The expansion of the exhaust gasses results in a supersonic jet.

The small particle sizes in STS leads to their low inertia or momentum, and this, combined with distinct particle temperatures and velocities, which are dependent on the particular technique used, can result in microstructures different to those of conventional thermal spray. Porous microstructures, which are of interest in this project, are produced when particles display low inertia so that they follow thermal flow lines close to the coating or substrate surface. This results in particles impacting the substrate at shallow angles, and subsequently acting as nucleation sites to build up the microstructure. An excess of nucleation sites results in the lack of a columnar microstructure, but typically high porosity, >20% (Aghasibeig, 2019).

Only a few papers were found on the production of CuO coatings using thermal spray processes, and only a subset of these studied the use of thermal spray to produce intentionally porous coatings. Asadi (2017) studied the influence of porous CuO structures on optical properties, but no information was presented in relation to the impact of processing parameters on porosity, and in fact the level of porosity was not quantified. CuO films, produced by spray pyrolysis, on porous silicon substrates have also been studied (Khashan, 2016; Chetoui, 2019).

TiO₂ thermal sprayed coatings have been studied more extensively and it was found that porosity was mainly influenced by the solution spray distance. A fragile porous structure was formed at long distances, 125mm, and denser structures produced at shorter distances (Vaßen, 2009). The phases produced after solution spraying were also influenced by temperature, with rutile favoured, over anatase under hotter conditions (Vaßen, 2009; Chen 2008). Gkomoza (2019) studied the influence of different powder processing routes and spray processes on porosity. It was found that flame spray, with plasma-atomised powders, produced the most porous structures (34% porous). The other combinations were plasma spray with plasma-atomised powders and plasma spray with hydride-dehydride powders.

A review of the boiling performance of thermal sprayed porous metallic coatings was conducted by Cieslinski (2011), who concluded that porous aluminium structures, on stainless steel tubes, showed superior performance relative to other materials (copper, brass, molybdenum, stainless steel), although all of the coated materials displayed superior performance, compared with a smooth tube. The performance advantage of coated small tube bundles, over smooth tube bundles, was independent of test liquid, pitch to diameter ratio, and pressure.

5.4 Ni-P/Ni-P-PTFE Coatings

Electroless nickel coatings are formed by dipping a substrate into a plating bath, which consists of a nickel salt and a reducing agent. Oxidation of the reducing agent occurs, which allows donation of electrons to the metal ions, in solution, and further allows deposition of the metal on the substrate. The process does not require an external current (Sudagar, 2017), and is auto-catalytic, so the deposition of the first layer of nickel acts as a catalyst for the rest of the process. Electroless nickel coatings are produced in baths mainly composed of nickel sulphate and sodium hypophosphate, which results in a deposited coating that is typically between 3-14% phosphorous. The phosphorous content can be controlled by variation of temperature, pH and bath composition. Lower pH, higher hypophosphate concentration in the solution and lower temperatures favour a higher phosphorous content. The density of the coating is also inversely proportional to the phosphorous content (Sudagar, 2013).

Electroless nickel is often utilised because of its excellent corrosion resistance good mechanical properties and reasonable cost. The composition of the coating, as well as the particular environment, can have a significant effect on corrosion resistance. High phosphorous coatings are favoured in environments containing phosphoric acid, i.e. acidic environments, while low phosphorous coatings are favoured in sodium hydroxide, i.e. alkaline, environments (Parkinson, 1997). Corrosion tests were undertaken on CS samples coated with Ni-P, with phosphorous content of 10.5%, at 25°C. Tests were undertaken for 250 hours with no noticeable material loss, or corrosive attack observed (Mainier, 2013).

There has been recent interest in the incorporation of particles into the Ni-P matrix, with hard particles co-deposited to improve wear performance (Sudagar, 2013). Ni-P-PTFE composite coatings have also been considered, and were found to have improved corrosion resistance as a result of sealing nano-pores (Wang, 2011). The presence of pinholes in Ni-P coatings has been noted as a concern for corrosion resistance in the oil and gas industry (Sudagar, 2013).

5.5 Amorphous metal coatings

Amorphous alloys, or metallic glasses, are metallic materials that lack long range crystallographic order, and are of significant interest as they can possess high strength, resistance to wear and corrosion performance. Generally glasses are formed by quenching, where the quench rate is so high that the nucleation of crystalline phases is inhibited. With such a high cooling rate the liquid enters a metastable supercooled state, below the melting temperature, and with further reductions in temperature the viscosity increases until it becomes a rigid glass, at the glass transition temperature (Jafary-Zadeh, 2018). The glass-forming ability (GFA) of an alloy is the minimum cooling rate for the production of a glass, and casting provides a fast enough cooling rate to allow the production of metallic glasses for alloys with good GFA. Physical vapour deposition (PVD) involves the condensation of gaseous particles onto a substrate with cooling rates of up to 10^{12} K/s, which allows deposition of amorphous alloys with lower GFA (Li, 2019).

Several possible factors that might be responsible for the good corrosion performance of amorphous alloys have been identified. These include the lack of grain boundaries and second phase particles, which are often sites for corrosion associated with denuded zones or galvanic effects (Scully, 2007). Alternatively, the metastable state of the alloy means that the alloy is highly chemically reactive. Therefore if the alloy has a high concentration of highly stable oxidising elements, that are able to impart a protective passive film, e.g. chromium, the passive film forms rapidly and is highly concentrated in the solute atoms (Hashimoto, 2011). Binary single-phase, chromium-containing, alloys have been studied, and it was determined that the corrosion resistance, in 12M HCl, of the binary amorphous alloys was generally better than for the pure metals. Cr-Ta amorphous alloys performed best, relative to alloys containing titanium, zirconium and niobium (Hashimoto, 2011). There has been limited study of amorphous alloys including tantalum and silicon, although some promising results have been obtained (Lai, 2018). The addition of silicon to Fe-Cr amorphous alloys is thought to improve corrosion resistance as SiO_2 passive films are formed (Souza, 2016). The corrosion rates of amorphous Fe-Cr-Ni-Ta and Cr-Ta alloys, in 12M HCl, were investigated and it was determined that the corrosion rates of both

amorphous alloys were lower than 304 stainless steel or bulk chromium. For both alloys there was a reduction of corrosion rate with increases in tantalum, but the Fe-Cr-Ni-Ta alloy appeared to show poorer corrosion performance relative to Cr-Ta (Li, 1999).

6. CORRELATIONS FOR POOL AND FLOW BOILING

A number of models have been proposed for correlation of critical heat flux with experimental data, These models are predominantly based on five different mechanisms, reviewed by Liang (2018) and Fang (2017):

- Bubble interference: Premised on the assumption that at high superheats the high bubble number and departure frequency causes bubbles to coalesce, separating liquid from heated surface. The key CHF equation related to this model is:

$$q_{CHF} = 0.012 \rho_g h_{lg} \left(\frac{\rho_f - \rho_g}{\rho_g} \right)^{0.6}$$

Where ρ_f and ρ_g are liquid and vapour density, respectively, and h_{lg} the latent heat of vaporisation.

- Macrolayer dryout: assumes a macrolayer of liquid underneath large mushroom shaped bubbles. CHF is triggered when the liquid macrolayer dries out, before bubble departure, leaving a dry heated surface. This model is expressed as:

$$q_{CHF} = \rho_f h_{lg} \delta \left(1 - \frac{A_g}{A_w} \right) f$$

Where δ , A_g and A_w are macrolayer thickness, area occupied by vapour jets and total surface area, respectively.

- Hydrodynamic instability: Considers CHF when the velocity of the vapour phases reaches a critical value:

$$q_{CHF} = \rho_g h_{lg} u_g \left(\frac{A_g}{A_w} \right)$$

Where u_g is vapour velocity. The hydrodynamic instability model is also commonly expressed as a dimensionless constant, K, which is usually assumed to be 0.131, as follows:

$$\frac{q_{CHF}}{\rho_g h_{lg} [\sigma g (\rho_f - \rho_g) / \rho_g^2]^{1/4}} = K = 0.131$$

Where σ and g are surface tension and acceleration due to gravity. This model has been modified to include the influence of surface roughness, pressure, liquid viscosity, surface roughness, wettability, i.e. contact angle, amongst other factors (Liang, 2018).

- Hot spot models: assumes small dry spots cover the heater surface during nucleate boiling and CHF occurs when liquid cannot be replenished at these growing dry spots.
- Interfacial lift-off: This model is based on flow boiling data and suggests a series of events before CHF is reached. Slightly below CHF, a vapour layer propagates along the surface and instability only permits liquid contact, with the heater surface, at distinct wave fronts. CHF occurs when the wetting wave fronts are lifted from the surface by the vapour beneath them (Galloway, 1993).

An extensive pool boiling database of CHF data, from smooth surfaces, was examined by Fang (2017) and it was determined that modified hydrodynamic instability models best matched the data, although even the best models had a deviation of ~27%. It was noted that the surface orientation was one of the most critical factors for CHF, and CHF decreased rapidly at between 90° and 180°, but was fairly insensitive to orientation between 0°, i.e. upward facing, and 90°.

A correlation for CHF of porous surfaces has been suggested, as follows:

$$q_{CHF} = 0.52 \varepsilon^{2.28} h_{lg} \sqrt{\sigma \rho_f \rho_g / (\rho_f + \rho_g) R_{br}}$$

Where ε is porosity and R_{br} the radius of vapour jets (Mori, 2017b). Cieslinski (2011) analysed flow boiling across porous surfaces to suggest another relationship:

$$\alpha = Cq^n$$

Where α is the heat transfer coefficient and the q heat flux. C and n are constants which are dependent on the refrigerant. This relationship is possibly the most appropriate for the GeoHex program, but its validity will be tested using the data generated in the program.

7. IMAGING METHODS FOR SIMULATION VALIDATION

In the GeoHex project simulation methods will be used to gain a better understanding of the bubble and droplet behaviour, as well as, to allow the prediction of the phenomena that are being studied under a wider range of flow speeds, temperatures and other factors. The developed tools will therefore allow simulation of coating performance, under various conditions, for which there might not be experimental data. As with most simulation techniques, validating the models with experimental data is a key concept. In the GeoHex program high-speed video (HSV) of the experiments will be recorded, processed and analysed, to validate the developed models. The footage will be used to compare the simulated bubble/droplet dynamics with actual behaviour during the experiments of condensation and boiling.

In order to develop accurate models of boiling and condensation heat transfer, the nucleation site density and the cycle of nucleation and growth must be accurately captured, and the temperature of the surfaces being tested must be accurately measured (Gerardi, 2010). Imaging of bubble dynamics is therefore very important for the development and validation of simulation tools. There are several ways to capture images of condensation and boiling. One way is to use high-speed conventional wavelength camera sensors, directly pointed at the surface being tested. These camera systems are usually tuned to allow shooting at high speeds, often in the order of magnitude of thousands of frames per second (FPS), without excessive sensitivity to surface lighting. This is important as the heat from surfaces can cause lighting and image distortions in heat transfer experiments. It should be noted that careful calibration of the imaging setup is important since the size of the droplets/bubbles in the footage will be measured based on pixel size and position. In other words, pixel size is converted into distance units and this introduces an uncertainty (Gerardi, 2010).

Infra-red (IR) cameras can be used to capture temperature measurements of the surface, without the need for thermocouples. Thermocouples tend to have slow response times and can only measure discreet points on the surface. These points might not, of course, coincide with bubble/condensate nucleation points.

In order to generate data on nucleation site density, bubble departure diameter and frequency, high speed video (HSV) footage of the condensation and boiling experiments will be taken, and the video will then be split into individual frames. The footage will then be analysed by computer vision (CV) tools, such as OpenCV library. This library includes methods for identifying the droplet/bubble nucleation sites, size, movement and other characteristics. This data will then be used to validate the simulations but will also be valuable in observing other characteristics of the coatings.

8. CONCLUSIONS

The characteristics of ideal boiling surfaces, for low surface tension fluids, were reviewed, as well as the specific processes that will be used in the GeoHex program and correlations between experimental data and heat transfer characteristics. The review identified that the main factors that enhance passive heat transfer performance, for ideal boiling surfaces, include:

- Increased numbers of active nucleation sites using micro- or nano-sized roughness;
- Wicking to allow rewetting of the structure and to allow fresh liquid to be delivered to the heated surface;
- Separation of vapour and liquid flow streams so that rewetting is not prevented because of vapour release. This includes sucking-evaporation mode surfaces, where evaporation causes sucking of liquid from networked inactive cavities.

Although there is consensus on these factors, knowledge on the engineering design of structures to achieve the above is lacking, and it is particularly unclear how engineered surfaces would behave with different fluid types, temperature and pressure, orientation, and when scaled to full size. Data on the longevity of performance, in representative environments, are also in question, particularly for micro- and nano-scale features that might be prone to clogging, as a result of corrosion or fouling, as well as erosion from abrasive media in fluids. It is therefore difficult to use the reviewed data for the design of structures and to inform design parameters. Design parameters will therefore be optimised with data obtained in the GeoHex program.

The review identified that there is a particular lack of data discussing the effect of process parameters on heat transfer and corrosion performance. There also appears to be a lack of long-term test data to prove the longevity of any coatings, and most studies investigated heat transfer enhancement with water as the working fluid, rather than fluids more appropriate for heat exchangers. Despite these deficiencies, the reviewed data will be useful as a starting point for the coating development in the GeoHex program, and the data generated by GeoHex will be a valuable addition to the current published literature.

9. REFERENCES

- Aghasibeg, M., Tarasi, F., Lima, R.S., Dolatabadi, A. and Moreau, C., 2019. A Review on Suspension Thermal Spray Patented Technology Evolution. *Journal of Thermal Spray Technology*, pp.1-27.
- Ahn, H.S., Sathyamurthi, V. and Banerjee, D., 2009. Pool boiling experiments on a nano-structured surface. *IEEE Transactions on components and packaging technologies*, 32(1), pp.156-165.
- Allred, T.P., Weibel, J.A. and Garimella, S.V., 2018. Enabling highly effective boiling from superhydrophobic surfaces. *Physical review letters*, 120(17), p.174501.
- Asadi, M. and Rozati, S.M., 2017. Optical and structural properties of nanostructured copper oxide thin films as solar selective coating prepared by spray pyrolysis method. *Materials Science-Poland*, 35(2), pp.355-361.
- Asano, H., Tomita, R., Inoue, M. and Takenaka, N. 2009, "Boiling heat transfer enhancement by thermal spray coating in a narrow channel", 5th Asian Conference on Refrigeration and Air Conditioning, ACRA 2010 - Green Breeze from Asia: Frontiers of Refrigerants, Heat Transfer and System.
- Attinger, D., Frankiewicz, C., Betz, A.R., Schutzius, T.M., Ganguly, R., Das, A., Kim, C.J. and Megaridis, C.M., 2014. Surface engineering for phase change heat transfer: A review. *MRS Energy & Sustainability*, 1, E4.
- Bejan, A. and Kraus, A.D. eds., 2003. *Heat transfer handbook* (Vol. 1). John Wiley & Sons.
- Calise, F., Macaluso, A., Pelella, P. and Vanoli, L., 2018. A comparison of heat transfer correlations applied to an Organic Rankine Cycle. *Engineering science and technology, an international journal*, 21(6), pp.1164-1180.
- Cieśliński, J.T., 2011. Flow and pool boiling on porous coated surfaces. *Reviews in Chemical Engineering*, 27(3-4), pp.179-190.
- Chen, D., Jordan, E.H. and Gell, M., 2008. Porous TiO₂ coating using the solution precursor plasma spray process. *Surface and Coatings Technology*, 202(24), pp.6113-6119.
- Chetoui, A. and Zouaoui, A., 2019. The spray-pyrolyzed copper oxide properties based precursor concentration. *Silicon*, 11(6), pp.3041-3048.
- Effendi, M., 2012. Effect of doping Fe on TiO₂ thin films prepared by spin coating method. *International Journal of Basic & Applied Sciences*, 12(02), pp.107-110
- Fang, X. and Dong, A., 2017. A comparative study of correlations of critical heat flux of pool boiling. *Journal of Nuclear Science and Technology*, 54(1), pp.1-12.
- Franco, A., Latrofa, E.M. and Yagov, V.V. 2006, "Heat transfer enhancement in pool boiling of a refrigerant fluid with wire nets structures", *Experimental Thermal and Fluid Science*, vol. 30, no. 3, pp. 263-275.
- Galloway, J.E. and Mudawar, I., 1993. CHF mechanism in flow boiling from a short heated wall. I: Examination of near-wall conditions with the aid of photomicrography and high-speed video imaging. *International journal of heat and mass transfer*, 36(10), pp.2511-2526.
- Gerardi, C., Buongiorno, J., Hu, L.W. and McKrell, T., 2010. Study of bubble growth in water pool boiling through synchronized, infrared thermometry and high-speed video. *International Journal of Heat and Mass Transfer*, 53(19-20), pp.4185-4192.

Date: 28 February 2020

Gkomoza, P., Lampropoulos, G.S., Vardavoulias, M., Pantelis, D.I., Karakizis, P.N. and Sarafoglou, C., 2019. Microstructural investigation of porous titanium coatings, produced by thermal spraying techniques, using plasma atomization and hydride-dehydride powders, for orthopedic implants. *Surface and Coatings Technology*, 357, pp.947-956.

Hashimoto, K., 2011. What we have learned from studies on chemical properties of amorphous alloys?. *Applied surface science*, 257(19), pp.8141-8150.

Jafary-Zadeh, M., Praveen Kumar, G., Branicio, P.S., Seifi, M., Lewandowski, J.J. and Cui, F., 2018. A critical review on metallic glasses as structural materials for cardiovascular stent applications. *Journal of functional biomaterials*, 9(1), p.19.

Khan, S., Atieh, M. and Koç, M., 2018. Micro-nano scale surface coating for nucleate boiling heat transfer: A critical review. *Energies*, 11(11), p.3189.

Khashan, K.S., Hassan, A.I. and Addie, A.J., 2016. Characterization of CuO thin films deposition on porous silicon by spray pyrolysis. *Surface Review and Letters*, 23(05), p.1650044.

Kingston, C.T. and Simard, B., 2003. Fabrication of carbon nanotubes. *Analytical Letters*, 36(15), pp.3119-3145.

Kumar, C.S., Suresh, S., Aneesh, C.R., Kumar, S., Praveen, A.S. and Raji, K., 2015. Flow boiling heat transfer enhancement on copper surface using Fe doped Al₂O₃-TiO₂ composite coatings. *Applied Surface Science*, 334, pp.102-109.

Kumar, C.S., Suresh, S., Praveen, A.S., Kumar, M.S. and Gopi, V., 2016. Effect of surfactant addition on hydrophilicity of ZnO-Al₂O₃ composite and enhancement of flow boiling heat transfer. *Experimental Thermal and Fluid Science*, 70, pp.325-334.

Kumar, C.S., Suresh, S., Yang, L., Yang, Q. and Aravind, S., 2014. Flow boiling heat transfer enhancement using carbon nanotube coatings. *Applied thermal engineering*, 65(1-2), pp.166-175.

Lai, J.J., Lin, Y.S., Chang, C.H., Wei, T.Y., Huang, J.C., Liao, Z.X., Lin, C.H. and Chen, C.H., 2018. Promising Ta-Ti-Zr-Si metallic glass coating without cytotoxic elements for bio-implant applications. *Applied Surface Science*, 427, pp.485-495.

Li, F.C., Liu, T., Zhang, J.Y., Shuang, S., Wang, Q., Wang, A.D., Wang, J.G. and Yang, Y., 2019. Amorphous-nanocrystalline alloys: fabrication, properties, and applications. *Materials Today Advances*, 4, p.100027.

Li, X.Y., Akiyama, E., Habazaki, H., Kawashima, A., Asami, K. and Hashimoto, K., 1999. The corrosion behavior of sputter-deposited amorphous Fe-Cr-Ni-Ta alloys in 12 M HCl. *Corrosion science*, 41(9), pp.1849-1869.

Liang, G. and Mudawar, I., 2018. Pool boiling critical heat flux (CHF)-Part 1: Review of mechanisms, models, and correlations. *International Journal of Heat and Mass Transfer*, 117, pp.1352-1367.

Liang, G. and Mudawar, I., 2019. Review of pool boiling enhancement by surface modification. *International Journal of Heat and Mass Transfer*, 128, pp.892-933.

Lin, C.Y.W., Channei, D., Koshy, P., Nakaruk, A. and Sorrell, C.C., 2012. Effect of Fe doping on TiO₂ films prepared by spin coating. *Ceramics International*, 38(5), pp.3943-3946.

Mainier, F.B., Fonseca, M.P.C., Tavares, S.S. and Pardal, J.M., 2013. Quality of electroless Ni-P (nickel-phosphorus) coatings applied in oil production equipment with salinity. *Journal of Materials Science and Chemical Engineering*, 1(6), pp.1-8.

Manawi, Y.M., Samara, A., Al-Ansari, T. and Atieh, M.A., 2018. A review of carbon nanomaterials' synthesis via the chemical vapor deposition (CVD) method. *Materials*, 11(5), p.822.

Mori, S. and Okuyama, K., 2017a. Critical heat flux enhancement using honeycomb porous plate in a saturated pool boiling of water-based nanofluid. 3th International Conference on Heat Transfer, Fluid Mechanics and Thermodynamics, Portoroz, Slovenia on 17-19 July 2017.

Mori, S. and Utaka, Y., 2017b. Critical heat flux enhancement by surface modification in a saturated pool boiling: a review. *International Journal of Heat and Mass Transfer*, 108, pp.2534-2557.

Mukherjee, S. and Mudawar, I., 2003. Pumpless loop for narrow channel and micro-channel boiling. *Journal of Electronic Packaging*, 125(3), pp.431-441.

Parkinson, R., 1997. Properties and applications of electroless nickel. Nickel Development Institute. Available from: <https://advancedplatingtech.com/wp-content/uploads/2013/10/Properties-and-Applications-of-Electroless-Nickel-R-Parkinson.pdf>, Accessed 21/02/2020

Pawlowski, L., 2008. Finely grained nanometric and submicrometric coatings by thermal spraying: A review. *Surface and Coatings Technology*, 202(18), pp.4318-4328.

Pialago, E.J.T., Kwon, O.K. and Park, C.W., 2013. Nucleate boiling heat transfer of R134a on cold sprayed CNT-Cu composite coatings. *Applied Thermal Engineering*, 56(1-2), pp.112-119.

Pioro, I.L., Rohsenow, W. and Doerffer, S.S., 2004. Nucleate pool-boiling heat transfer. I: review of parametric effects of boiling surface. *International Journal of Heat and Mass Transfer*, 47(23), pp.5033-5044.

Rahman, M.M., Olceroglu, E. and McCarthy, M., 2014. Role of wickability on the critical heat flux of structured superhydrophilic surfaces. *Langmuir*, 30(37), pp.11225-11234.

Rahman, M.M., Pollack, J. and McCarthy, M., 2015. Increasing boiling heat transfer using low conductivity materials. *Scientific reports*, 5, p.13145.

Scully, J.R., Gebert, A. and Payer, J.H., 2007. Corrosion and related mechanical properties of bulk metallic glasses. *Journal of Materials Research*, 22(2), pp.302-313.

Sheikholeslami, M., Gorji-Bandpy, M. and Ganji, D.D., 2015. Review of heat transfer enhancement methods: Focus on passive methods using swirl flow devices. *Renewable and Sustainable Energy Reviews*, 49, pp.444-469.

Singh, N., Sathyamurthy, V., Peterson, W., Arendt, J. and Banerjee, D., 2010. Flow boiling enhancement on a horizontal heater using carbon nanotube coatings. *International Journal of Heat and Fluid Flow*, 31(2), pp.201-207.

Souza, C.A.C., Ribeiro, D.V. and Kiminami, C.S., 2016. Corrosion resistance of Fe-Cr-based amorphous alloys: An overview. *Journal of Non-Crystalline Solids*, 442, pp.56-66.

Sudagar, J., Lian, J. and Sha, W., 2013. Electroless nickel, alloy, composite and nano coatings-A critical review. *Journal of Alloys and Compounds*, 571, pp.183-204.

Sudagar, J., Tamilarasan, R., Sanjith, U., Rajendran, R. and Kumar, R., 2017. Electroless Deposition of Nanolayered Metallic Coatings. *Nanoscaled Films and Layers*, p.27.

Sulzer Metco, 2013. An Introduction to Thermal Spray. Available from: https://www.upc.edu/sct/es/documents_equipamento/d_324_id-804-2.pdf, accessed 04/02/20

Thulukkanam, K., 2013. Heat exchanger design handbook. CRC press.

Toma, F.L., Berger, L.M., Langner, S. and Naumann, T., 2010. Suspension Spraying—The Potential of a New Spray Technology, *Therm. Spray Bull*, 3(1), pp.24-29.

Document: D1.3 Ideal flow boiling surface for ORC

Version: 1.0

Date: 28 February 2020

Vaßen, R., Yi, Z., Kaßner, H. and Stöver, D., 2009. Suspension plasma spraying of TiO₂ for the manufacture of photovoltaic cells. *Surface and Coatings Technology*, 203(15), pp.2146-2149.

Vlachou, M.C., Lioumbas, J.S. and Karapantsios, T.D., 2015. Heat transfer enhancement in boiling over modified surfaces: A critical review. *Interfacial Phenomena and Heat Transfer*, 3(4).

Wang, X.D., Vinodgopal, K. and Dai, G.P., 2019. Synthesis of Carbon Nanotubes by Catalytic Chemical Vapor Deposition. In *Perspective of Carbon Nanotubes*. IntechOpen.

Wang, J., Tian, J., Liu, X., Yin, Y. and Wang, X., 2011. Effect of polytetrafluoroethylene content on electrochemical anticorrosion behaviors of electroless deposited Ni-P and Ni-P-polytetrafluoroethylene coatings in seawater. *Thin Solid Films*, 519(18), pp.5905-5911.

Weng, W., Ma, M., Du, P., Zhao, G., Shen, G., Wang, J. and Han, G., 2005. Superhydrophilic Fe doped titanium dioxide thin films prepared by a spray pyrolysis deposition. *Surface and Coatings Technology*, 198(1-3), pp.340-344.

Yang, Y., Ji, X. and Xu, J., 2010. Pool boiling heat transfer on copper foam covers with water as working fluid. *International Journal of Thermal Sciences*, 49(7), pp.1227-1237.

Zheng, X. and Park, C.W., 2015. Experimental study of the sintered multi-walled carbon nanotube/copper microstructures for boiling heat transfer. *Applied Thermal Engineering*, 86, pp.14-26.

Zhong, D., Meng, J.A., Li, Z. and Guo, Z., 2015. Critical heat flux for downward-facing saturated pool boiling on pin fin surfaces. *International Journal of Heat and Mass Transfer*, 87, pp.201-211.